Global Bifurcation to Traveling Waves in Axisymmetric Convection

Laurette S. Tuckerman and Dwight Barkley
Department of Physics and Center for Nonlinear Dynamics, University of Texas, Austin, Texas 78712
(Received 25 January 1988)

A traveling-wave state observed in full numerical simulations of cylindrical convection is reported. These waves arise with large amplitude via a global bifurcation of the steady convective state in systems with highly conducting sidewalls. For poorly conducting sidewalls, transition occurs instead to a disconnected branch of steady states. The Prandtl-number dependence of these transitions is interpreted in light of a wavelength selection mechanism previously proposed for axisymmetric convection.

PACS numbers: 47.20.Ky, 47.25.Qv

Many recent studies of Rayleigh-Bénard convection have focused on time-dependent spatial patterns. Theory and experiment agree regarding the existence of traveling-wave solutions in binary fluids[1] and in systems with spatially ramped Rayleigh number.[2,3] Traveling waves have also been predicted, both analytically[4] and with model equations,[5] to occur in axisymmetric convection; these, however, have never been observed experimentally.

We report here on observations of axisymmetric traveling waves near the onset of convection in simulations of the full time-dependent Boussinesq equations for a cylindrical geometry. We find that these waves, for sufficiently high Prandtl number, are not subject to the nonaxisymmetric instabilities often observed,[6] but significantly, that they are suppressed when the sidewalls have the poor conductivity typical of past experiments. Along with detailed quantitative predictions, we present a description of the global bifurcation triggering these waves, and a simple model which reproduces the parameter dependence of this bifurcation.

We have obtained our results using an initial-value pseudospectral code, which has additional capabilities for calculating unstable steady states and eigenvectors.[7] All computations have been performed for aspect ratio $\Gamma=5$, with use of fifty Chebyshev polynomials in the radial direction r, sixteen polynomials in the vertical direction z, and a time step of 0.002. (All times are expressed in units of the vertical thermal diffusion time $t_v=d^2/\kappa$, where d and κ are the depth and thermal diffusivity of the fluid layer; all distances are expressed in units of d.)

The top and bottom plates are perfect thermal conductors. We have investigated both thermally conducting and insulating sidewalls, corresponding to Dirichlet ($h=0$) and Neumann ($\partial_r h=0$) boundary conditions, respectively, where h is the temperature deviation from the conductive profile. All boundaries are rigid: Boundary conditions $u_r=u_z=0$ are imposed on the velocity. The boundary conditions and equations are reflection symmetric about the midplane $z=0$.

The most detailed results reported here are for $N_{\mathrm{Pr}}=10$. For this Prandtl number and aspect ratio $\Gamma=5$, and in the range of Rayleigh number studied, we have determined that, once obtained, axisymmetric patterns[8] are stable to nonaxisymmetric perturbations of the form $\exp(im\theta)$ for all $m\leq 5$. We have tested the stability of the steady states by determining that the most unstable nonaxisymmetric eigenvector has a negative growth rate, and that of the periodic states by observing the decay of nonaxisymmetric perturbations in full three-dimensional nonlinear simulations. We shall also present some results for a wide range of Prandtl numbers, including some ($N_{\mathrm{Pr}}\lesssim 4$) for which we have found the system to be unstable to a nonaxisymmetric perturbation with $m=1$.

We now describe two bifurcation sequences (one for

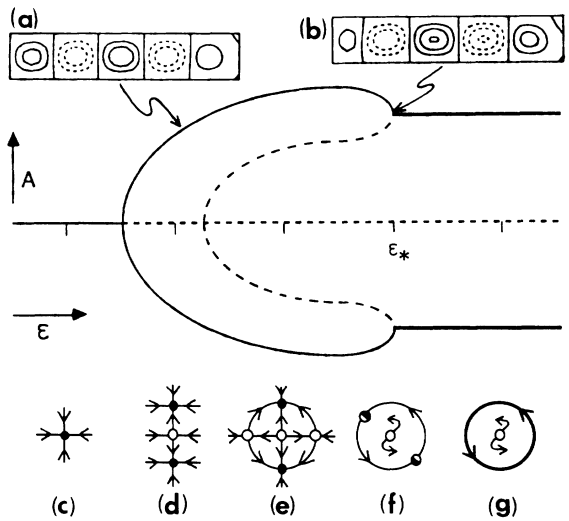

FIG. 1. Schematic bifurcation diagram for the case of conducting sidewalls. ϵ is the reduced Rayleigh number, and A is a coordinate which distinguishes between different states. (a),(b) Numerically calculated stream function contours of representative five-roll steady states at two values of ϵ. (c)–(g) Phase portraits at the five values of ϵ denoted by tick marks. Stable (unstable) states are denoted by solid (dashed) lines in the bifurcation diagram, and by filled (empty) circles in the phase portraits. The traveling-wave state (see Fig. 2) is denoted by bold lines.

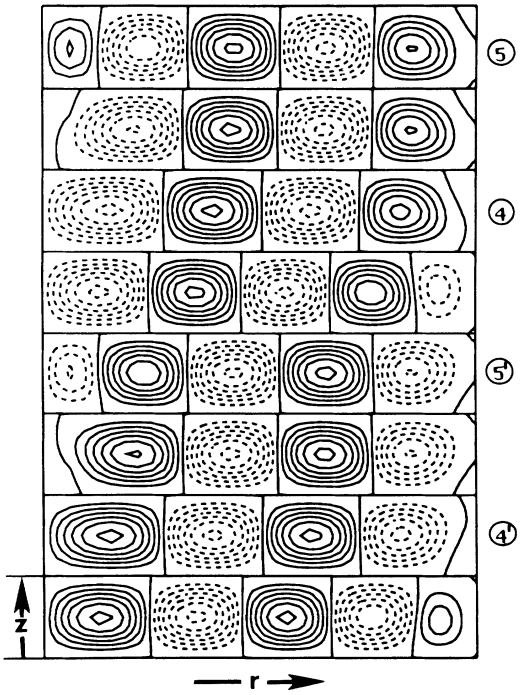

FIG. 2. Instantaneous stream function contours in the r-z plane of the traveling-wave state at $\epsilon=1.39$. Solid (dashed) contours denote clockwise (counterclockwise) flow. Contours are shown at times $t=0$, 19, 27, 34, 70, 89, 97, and 104. The numbers label slowly varying quasi five-roll and quasi four-roll states.

conducting sidewalls and one for insulating sidewalls) as a function of reduced Rayleigh number $\epsilon \equiv (R-R_c)/R_c$, where R_c is the critical Rayleigh number for onset of convection. For $\Gamma=5$, $R_c=1734$, as found previously by numerical linear stability analysis[9] and confirmed by us to within 0.1%.

A schematic bifurcation diagram summarizing our findings for the case of conducting sidewalls is shown in Fig. 1. For negative ϵ the conductive state is stable [Fig. 1(c)]. At $\epsilon=0$, a supercritical bifurcation breaks the reflection symmetry, giving rise to two symmetrically related steady five-roll states [Fig. 1(d)]. Figure 1(a) shows numerically obtained stream functions in the r-z plane for one of these two states. As ϵ is increased, the size of the central roll [the leftmost roll in Figs. 1(a) and 1(b)] decreases, until at a critical value $\epsilon_*=1.3844 \pm 0.0002$ the stable five-roll state gives way to a large-amplitude low-frequency traveling wave (limit cycle), indicated with bold lines in Fig. 1.

Instantaneous stream functions for the traveling-wave state are shown in Fig. 2 for $\epsilon=1.39$. The central roll grows smaller and is annihilated, while new rolls are continually created at the sidewall, leading, heuristically, to alternation between four and five rolls. Note that the transition to periodic behavior is a *symmetry-restoring* bifurcation, as the states in the second half of the limit cycle are related by z reflection to those of the first half.

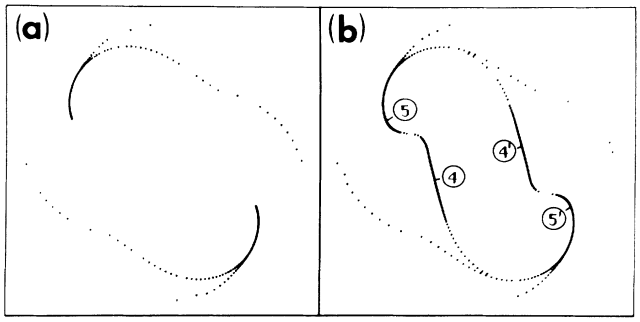

FIG. 3. Numerically computed phase portraits at (a) $\epsilon=1.38$ [corresponding to Fig. 1(f)] and at (b) $\epsilon=1.39$ [traveling-wave state of Fig. 1(g) and Fig. 2]. The coordinates are the projections onto the two most unstable eigenvectors of the conductive state (at $\epsilon=1.40$). Trajectories emanating from four different initial conditions are shown in each case. Points are equally spaced in time. All trajectories in (a) terminate at one of two steady states. Numbers in (b) refer to Fig. 2.

The period of the oscillations diverges at onset: The periods at $\epsilon=1.3846$, 1.39, and 2.00 are 492, 140, and 25, respectively. In addition, the traveling waves are born with finite amplitude, indicating that they arise from a global (heteroclinic) bifurcation, rather than a Hopf bifurcation. The scenario leading up to the formation of the traveling-wave state is as follows. After the first supercritical bifurcation [Fig. 1(d)], the conductive branch undergoes a second supercritical bifurcation to a pair of *unstable* five-roll states [Fig. 1(e)]. These new unstable states inherit from the conductive state trajectories that terminate on the stable five-roll states.

The onset of periodic behavior is marked by the collision of the unstable and stable states in a pair of saddle-node bifurcations [Fig. 1(f)]; the connections between these steady states form the heteroclinic orbit. We have verified the existence of the saddle-node bifurcation by determining that the least stable eigenvalue along the stable five-roll branch goes to zero as $(\epsilon_*-\epsilon)^{1/2}$. We have confirmed its role in the formation of the traveling-wave state by numerically generating phase portraits before [Fig. 3(a)] and after [Fig. 3(b)] the saddle-node bifurcation [compare with Figs. 1(f) and 1(g)]. The system evolves very slowly as it passes "ghosts" of the five-roll states labeled 5 and 5'.

We now turn to the case of insulating sidewalls, again summarizing our findings in a schematic bifurcation diagram (Fig. 4). Traveling waves are not observed. Upon an increase of ϵ, the primary five-roll branch again loses stability via a saddle-node bifurcation, at a value $\epsilon_*=1.4115$ quite close to the transition point $\epsilon_*=1.3844$ for conducting sidewalls. However, this time the transition is to another *steady state*, one having four rolls [Fig. 4(a)]. The transition is strongly hysteretic: The four-

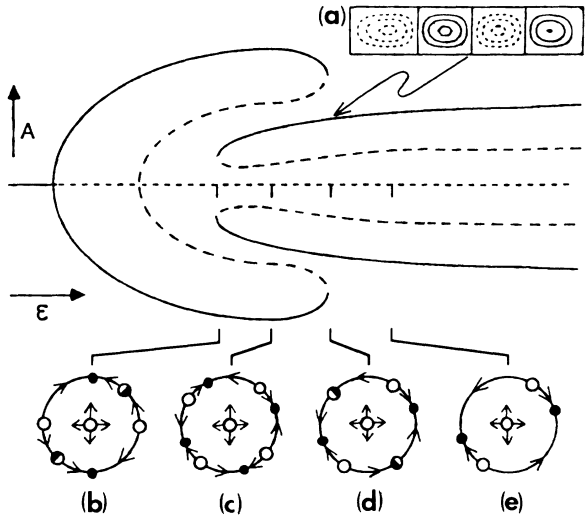

FIG. 4. Schematic bifurcation diagram for the case of insulating sidewalls. Conventions are the same as in Fig. 1. The diagram differs from Fig. 1 by the absence of the traveling-wave state and by the presence of additional steady four-roll states (a).

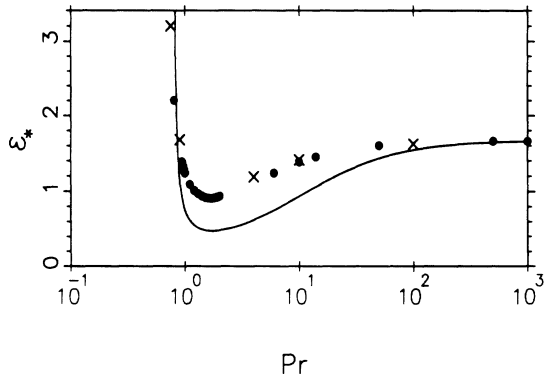

FIG. 5. The value ϵ_* of the saddle-node bifurcation terminating the five-roll branch plotted as a function of Prandtl number, denoted in the figure by Pr. The circles and crosses refer to conducting and insulating boundaries, respectively. The solid curve is the solution to the equation $\lambda(\epsilon_*', N_{Pr})$ =const, where $\lambda(\epsilon_*', N_{Pr})$ is given by the wavelength selection criterion of Manneville and Piquemal (Ref. 13), and the constant is chosen to match the curve to our data at $N_{Pr}=1000$. Both ϵ_*' and ϵ_* attain their minimum at $N_{Pr}=1.7$ and climb steeply at low N_{Pr}. For water ($N_{Pr}\approx 6$), $\epsilon_*=1.24$.

roll branch can be followed by decreasing ϵ until it disappears via a saddle-node bifurcation (of Eckhaus[10] type) at $\epsilon\approx 0.1$, inducing a transition back to the primary five-roll branch. (We have also followed this four-roll branch to values of ϵ as high as 6.0.) The phase portraits [Figs. 4(b)–4(e)] illustrate the emergence of the four-roll states, which intercept the trajectories in such a way as to prevent the formation of the limit cycle. Note that the "ghosts" of these four-roll states influence the dynamics even when the sidewalls are conducting, causing the slow regions 4 and 4′ in the limit cycle of Fig. 3(b).

Axisymmetric traveling waves such as we described above have never been observed experimentally. To understand this, we have investigated the hybrid boundary condition[11] $\mu h+\partial_r h=0$, which for $\mu\equiv(\pi\kappa_w/\kappa)\times\tanh(\pi t_w)$ approximates sidewalls with a finite thermal diffusivity κ_w and thickness t_w. Our simulations show that, for N_{Pr} near 10 and Γ near 5, traveling waves should occur in an experimental apparatus only when $\mu>33$. Thus it is because experiments have heretofore been conducted with $\mu\sim 1$ that these waves have remained unobserved.

Our results are in accord with a prediction[11] that the band of roll sizes allowed in *steady* convection is narrower for conducting than for insulating sidewalls. This prediction is supported by a numerical simulation of the Boussinesq equations in a rectangular container.[12]

We have also examined the Prandtl-number dependence (see Fig. 5) of the critical value ϵ_* marking the termination of the five-roll branch. (These points provide experimental predictions only for $N_{Pr}\gtrsim 5$, since we have determined that axisymmetric flows are unstable at lower Prandtl numbers.) For all values of N_{Pr}, as ϵ is increased to ϵ_*, we have found that the four noncentral rolls expand at the expense of the central roll, as shown in Figs. 1(a) and 1(b), and that the five-roll states corresponding to points in Fig. 5 have a small central roll of approximately the same size. This suggests a simple model for the transition: There exists some size δ, independent of N_{Pr} and μ, below which the central roll cannot survive, but instead vanishes abruptly (the same phenomenon causes a saddle-node bifurcation in spherical Couette flow[14]).

A second ingredient of our model comes from a theory of axisymmetric wavelength selection[4,13,15] which predicts the size λ of rolls as a function of ϵ and N_{Pr}. Let us assume that the sizes of the four outermost rolls are determined by the wavelength selection mechanism. With the hypothesis of a minimum central-roll size δ, we predict that the five-roll branch terminates when $4\lambda(\epsilon_*,N_{Pr})+\delta=5$. This yields an implicit equation for $\epsilon_*'(N_{Pr})$, the transition point predicted by our model. We plot $\epsilon_*'(N_{Pr})$ calculated from the analytic expression of Manneville and Piquemal[13] as the solid curve in Fig. 5. Although ϵ_*' is derived from an asymptotic expansion in ϵ and in $1/r$, it reproduces the most visible features of our points extremely well.

While we have used wavelength selection to gain physical insight, this approach cannot predict the range of phenomena we observe: The role of the wavelength selection mechanisms is complementary to that of full numerical simulation. Midway between the two lie theories of phases dynamics,[16] which seek a reduced set

of dynamical equations. Some authors,[2,4] relating time dependence to pattern frustration, have indeed used phase dynamics to predict, qualitatively, slow traveling waves caused by incompatible wavelength selection mechanisms operating at different spatial locations.

In conclusion, we have shown that by employing sidewalls of sufficiently high thermal conductivity, it is possible to obtain axisymmetric traveling waves in a cylindrical geometry. We have analyzed the global bifurcation giving rise to these waves and the Prandtl-number dependence of this bifurcation. We hope that our quantitative analysis will stimulate experimental investigation of these waves.

We thank M. Schumaker, and also A. Arneodo, V. Croquette, P. Le Gal, H. L. Swinney, and J. Vastano for helpful discussions. This research was supported by the National Science Foundation Division of Mathematical Sciences, the U.S. Office of Naval Research Nonlinear Dynamics Program, and the Center for Statistical Mechanics. Computing resources for this work were provided by the University of Texas Center for High Performance Computing.

[1]R. W. Walden, P. Kolodner, A. Passner, and C. M. Surko, Phys. Rev. Lett. **55**, 496 (1985); E. Knobloch, Phys. Rev. A **34**, 1538 (1986).

[2]L. Kramer, E. Ben-Jacob, H. Brand, and M. C. Cross, Phys. Rev. Lett. **49**, 1891 (1982).

[3]I. Rehberg, E. Bodenschatz, B. Winkler, and F. H. Busse, Phys. Rev. Lett. **59**, 282 (1987).

[4]Y. Pomeau and P. Manneville, J. Phys. (Paris) **42**, 1067 (1981).

[5]Y. Pomeau, S. Zaleski, and P. Manneville, Z. Angew. Math. Phys. **36**, 367 (1985).

[6]V. Croquette, P. Le Gal, A. Pocheau, and R. Guglielmetti, Europhys. Lett. **1**, 393 (1986); V. Steinberg, G. Ahlers, and D. S. Cannell, Phys. Scr. **T9**, 97 (1985).

[7]C. Canuto, M. Y. Hussaini, A. Quateroni, and T. A. Zang, *Spectral Methods in Fluid Dynamics* (Springer-Verlag, Berlin, 1987); P. S. Marcus and L. S. Tuckerman, J. Fluid Mech. **185**, 1 (1987); L. S. Tuckerman, to be published.

[8]E. L. Koschmieder and S. G. Pallas, Int. J. Heat Mass Transfer **17**, 991 (1974).

[9]G. S. Charlson and R. L. Sani, Int. J. Heat Mass Transfer **13**, 1479 (1970).

[10]V. Eckhaus, *Studies in Nonlinear Stability Theory* (Springer-Verlag, Berlin, 1965).

[11]M. C. Cross, P. G. Daniels, P. C. Hohenberg, and E. D. Siggia, J. Fluid Mech. **127**, 155 (1983).

[12]J. C. Mitais, P. Haldenwang, and G. Labrosse, in *Proceeding of the Eighth International Heat Transfer Conference*, edited by C. L. Tien, V. P. Carey, and J. K. Ferell (Harper and Row, New York, 1986).

[13]P. Manneville and J. M. Piquemal, Phys. Rev. A **28**, 1774 (1983).

[14]P. S. Marcus and L. S. Tuckerman, J. Fluid Mech. **185**, 31 (1987).

[15]M. C. Cross, Phys. Rev. A **27**, 490 (1983); J. C. Buell and I. Catton, Phys. Fluids **29**, 23 (1986).

[16]M. C. Cross and A. C. Newell, Physica (Amsterdam) **10D**, 299 (1984).